Seasonal variations of mass absorption efficiency of elemental carbon in $PM_{2.5}$ in urban Guangzhou of south China

Chenglei Pei[1,2,3,4], Yunfei Wu[5,*], Jun Tao[6,*], Leiming Zhang[7], Tao Zhang[1,2,3,8], Runqi Zhang[1,2,3], Sheng Li[1,2,3]

1. State Key Laboratory of Organic Geochemistry and Guangdong Key Laboratory of Environmental Protection and Resources Utilization, Guangzhou Institute of Geochemistry, Chinese Academy of Sciences, Guangzhou 510640, China
2. CAS Center for Excellence in Deep Earth Science, Guangzhou 510640, China
3. University of Chinese Academy of Sciences, Beijing 100049, China
4. Guangzhou Sub-branch of Guangdong Ecological and Environmental Monitoring Center, Guangzhou 518049, China
5. Key Laboratory of Middle Atmosphere and Global Environment Observation, Institute of Atmospheric Physics, Chinese Academy of Sciences, Beijing 100029, China
6. Institute for Environmental and Climate Research, Jinan University, Guangzhou 510632, China
7. Air Quality Research Division, Science and Technology Branch, Environment and Climate Change Canada, Toronto, Canada
8. Guangdong Ecological and Environmental Monitoring Center, Guangzhou 510308, China

---

*Corresponding authors: (Yunfei Wu) wuyf@mail.iap.ac.cn; (Jun Tao) taojun@jnu.edu.cn

Abstract: This study investigates seasonal variations of mass absorption efficiency of elemental carbon (MAE_{EC}) and possible influencing factors in urban Guangzhou of south China. Mass concentrations of elemental carbon (EC) and organic carbon (OC) in $PM_{2.5}$ and aerosol absorption coefficient (b_{ap}) at multi-wavelengths were simultaneously measured in four seasons of 2018–2019 at hourly resolution by a semi-continuous carbon analyzer and an aethalometer. Seasonal average mass concentrations of EC were in the range of 1.36–1.70 μgC/m^3 with a lower value in summer than in the other seasons, while those of OC were in the range of 4.70–6.49 μgC/m^3 with the lowest value in summer and the highest in autumn. Vehicle exhaust from local traffic was identified to be the predominant source of carbonaceous aerosols. The average aerosol absorption Ångström exponents (*AAE*) were lower than 1.2 in four seasons, indicating EC and b_{ap} were closely related with vehicle exhaust. Seasonal MAE_{EC} at 550 nm was 11.0, 8.5, 10.4 and 11.3 m^2/g in spring, summer, autumn, and winter, respectively. High MAE_{EC} was related with the high mass ratio of non-carbonaceous aerosols to EC and high ambient relative humidity.

Keywords: vehicle exhaust; non-carbonaceous aerosols; absorption enhancement; relative humidity

Introduction

Elemental carbon (EC), also termed as black carbon (BC) from an optical perspective, is the most crucial light absorption matter in atmospheric aerosols (Andreae and Gelencsér, 2006). EC poses direct warming effect (Bond et al., 2013), and also affects visibility and atmospheric stability due to its strong absorption of solar radiation (Ding et al., 2016; Jia et al., 2021; Luo et al., 2021). EC deposited onto snow surface also plays an essential role in the weather and climate system over the Tibetan Plateau (Zhao et al., 2020). Thus, knowledge of the optical properties of EC at high temporal resolution in different environments is needed to address air quality and climate issues. One of the key optical properties of EC is its mass absorption efficiency (MAE_{EC}), which is an essential parameter for estimating the contribution of EC to light absorption coefficient (b_{ap}) of atmospheric aerosols. A constant MAE_{EC} value of 6.5 m^2/g at 550 nm was recommended by the US IMPROVE (Interagency Monitoring of Protected Visual Environments) observation network (Tao et al., 2020). In fact, a wide range of MAE_{EC} value has been reported due to different mixing states of EC with coating aerosols (Cappa et al., 2012; Lack and Cappa, 2010; Peng et al., 2016; Wang et al., 2017, 2019; Wu et al., 2016b; Xie et al., 2019a, 2019b; Zhang et al., 2018). Theoretically, MAE_{EC} would be enhanced by a factor of 2.0 when an EC particle is fully coated by non-absorbing materials with a shell to core diameter ratio as large as 2.8 (Zhang et al., 2017). The dependence of bulk MAE_{EC} in fine particle ($PM_{2.5}$) on the mass ratio of non-absorbing materials to EC is weaker in cleaner than polluted environment where EC emissions are dominated by vehicle exhaust (Cappa et al., 2012, 2019; Lan et al., 2013), mainly because only a small fraction of EC was well coated by non-absorbing materials in real world. Size distribution of EC is another important factor influencing MAE_{EC}, e.g., MAE_{EC} could decrease by approximately 6% if the mass median diameter of EC increased from 140 nm to 200 nm (Zhang et al., 2018).

Benefited from a series of emission control measures across China, annual mass concentrations of $PM_{2.5}$ in the Pearl River Delta (PRD) region in south China have

decreased evidently since a decade ago and met the national air quality standard (< 35 μg/m^3) for many years. However, mass concentrations of EC in $PM_{2.5}$ have not evidently decreased compared to the case of secondary inorganic aerosols (SIAs, e.g., sulfate and nitrate) and organic carbon (OC) due to the large number of vehicle population in urban areas in this region (Tao et al., 2017a). Recently, continuous decreases in OC and sulfate concentrations while an elevation of nitrate concentration and its fraction in $PM_{2.5}$ were observed in urban Guangzhou, a megacity of the PRD region (Li et al., 2021). The change of chemical compositions has already affected the physical and optical properties of $PM_{2.5}$ in this region, e.g., increased the hygroscopicity (Xu et al., 2020; Li et al., 2021). Different change patterns of SIA species and OC, despite the flat EC mass concentration in recent years, certainly would affect MAE_{EC} in this region. However, previous studies mainly focused on the impact of atmospheric aging process and deliquescence of aerosol under the high ambient RH on MAE_{EC} in this region (Sun et al., 2020; Tao et al., 2021). The impact of changes of non-absorbing materials (SIAs and OC) relative to EC on MAE_{EC} has yet to be validated in this region.

To shed some light on the causes of seasonal variations in MAE_{EC}, a measurement campaign was conducted in an urban environment in Guangzhou in April, July and October of 2018 and January of 2019, which represent four different seasons. During the campaign, hourly mass concentrations of organic carbon (OC), EC, b_{ap}, criteria air pollutants and meteorological parameters were collected. In the following sections, mass concentrations and potential sources of carbonaceous aerosols were first characterized (Section 2.1), aerosol absorption coefficient and its wavelength dependence were then analyzed (Section 2.2), and finally seasonal variations in MAE_{EC} and associated influencing factors were explored (Section 2.3). Knowledge gained from this study is useful in evaluating visibility degradation and regional climate change in South China.

1 Methodology

1.1 Sampling site

The measurement campaign was conducted at a national air quality monitoring site located on the roof of a seven-story building inside the original Guangzhou Environmental Monitoring Center (GEMC) (23.13°N, 113.26°E) in Guangzhou (**Fig. 1**). There are no obvious industrial emissions within 10 km surrounding the site, but the site is affected by local sources such as traffic and residential activities. The site can be considered to represent typical urban environment in this city. Mass concentrations of EC (C_{EC}) and OC (C_{OC}) and b_{ap} were measured in April, July and October 2018 and January 2019, representing spring, summer, autumn and winter, respectively.

1.2 Online measurement of EC and OC mass concentrations

A model RT-4 Sunset semi-continuous carbon analyzer (Sunset Laboratory Inc, OR, USA) was utilized to measure C_{EC} and C_{OC} with a time resolution of 1 hr. Ambient air, after passing a $PM_{2.5}$ cutoff inlet, was drawn into the carbon analyzer via a 2 m stainless steel tube by the internal pump at a flow rate of 8 L/min. A denude was installed in front of the carbon analyzer to trap volatile OC. Fine particles were retained on a quartz filter in the first 45 min of each hour, and then delivered into a quartz furnace for OC and EC analysis in the next 15 min using the thermo-optical approach. OC was first vaporized by stepwise heating in a pure helium (He) environment. Subsequently, oxygen was mixed (2% O_2 in He) to oxidize EC on the filter. The decomposition products of the above two steps were detected by a flame ionization detector to quantify the carbon amounts. During the analysis, a laser beam continuously irradiated the quartz filter. When OC was carbonized with the elevated temperature under the pure He environment, the intensity of transmitted light of the laser gradually decreased. Subsequently, the transmitted light progressively increased with the oxidation and decomposition of carbonized OC and EC under the He/O_2 environment. The moment when the transmitted light was back to its initial intensity was defined as the split point to discriminate OC and EC. The carbon amounts detected before this split point was defined as OC, and that detected afterwards was defined as EC. Operation principle of the carbon analyzer was described in detail by (Birch and Cary, 1996). The semi-

continuous carbon analyzer was calibrated with the above-mentioned three sets of sucrose standard solutions (0.5, 1.0 and 2.0 ppm) once in every three days. The uncertainties of this measurement system were generally less than 10% according to the calibration curves.

1.3 Online measurement of the aerosol absorption coefficient

A model AE-31 aethalometer (Magee Scientific, CA, USA) was used to obtain b_{ap} at seven wavelengths of 370, 470, 520, 590, 660, 880 and 950 nm with a time resolution of 5 min. The aethalometer was also equipped with a $PM_{2.5}$ cutoff inlet to ensure only fine particles were measured. Meanwhile, a heating device (controlled at a constant temperature of 50℃) was installed in front of the aethalometer to dry the sample. Note that the heating device might evaporate a very small amount of coating materials and slightly reduce light attenuation. The value of b_{ap} can be obtained from the measured attenuation (*ATN*) together with equations (1), (2) and (3), as described in Weingartner et al. (2003):

$$b_{ap} = \frac{ATN}{t} \cdot \frac{A}{Q} \cdot \frac{1}{R(ATN) \cdot C} \quad (1)$$

$$R = \left(\frac{1}{f} - 1\right) \cdot \frac{ln(ATN) - ln(10)}{ln(50) - ln(10)} + 1 \quad (2)$$

$$f = \alpha(1 - \omega) + 1 \quad (3)$$

where t is the sampling time for a single measurement, A is the sampling area on the filter membrane, and Q is the sampling flow rate which was set as 5 L/min in this study. The Q value was routinely checked using a Gilibrator-2 flowmeter (Sensidyne, USA) once in every month, which showed deviations of less than 5% from the preset value throughout the study period. C and R in Eq. (1) are the two factors introduced to correct the inherent errors in b_{ap} determination using the AE-31 aethalometer. Factor C is used to correct the scattering effect of filter membrane and laden particles which was set as a constant of 3.5 as recommended by WMO (Xia et al., 2020). This value is also close to that derived by comparing AE-31 measured attenuation coefficient with the reference b_{ap} obtained by a multi-angle absorption photometer (MAAP) (Wu et al., 2021). Factor

129 R as a function of ATN is employed to correct the loading effect (Weingartner et al.,
130 2003). The variable ω in Eq. (3) represents the single scattering albedo which was set
131 as a mean value of 0.83 in Guangzhou (Andreae et al., 2008), and α is a constant scale
132 factor which was set as 0.86 in this study (Weingartner et al., 2003). Zero checks were
133 performed once in every season (three months) by installing a high efficiency filter
134 before the inlet of the aethalometer, which can remove most particles in the sample air.
135 There was no obvious deviation of the measured value from zero. The measurement
136 uncertainty of aethalometer were less than 5% as claimed by the manufacturer.
137 However, some empirical corrections were induced in the b_{ap} calculation which likely
138 enlarged the uncertainty of the determined b_{ap}.

139 b_{ap} generally exhibits as a power-law function of wavelength (λ), the exponent of
140 which is defined as absorption Ångström exponent (*AAE*):

141 $$b_{ap,\lambda} \propto \lambda^{-AAE} \quad (4)$$

142 In this study, the *AAE* value is derived from the linear regression of the obtained
143 b_{ap} against the seven wavelengths in the range of 370–950 nm on a logarithm scale,
144 thereby denoted as $AAE_{370\text{-}950nm}$.

145 **1.4 Auxiliary measurements for air pollution and meteorological parameters**

146 Mass concentrations of $PM_{2.5}$ and mixing ratios of gaseous pollutants including
147 SO_2, NO_2, NO, CO and O_3 were obtained from a co-located national air quality station.
148 An automatic weather station (Vaisala Co., Ltd.， Finland) was deployed to provide
149 meteorological data including wind speed, wind direction, temperature, relative
150 humidity (RH) and air pressure.

151 **2 Results and discussion**

152 **2.1 Mass concentrations and potential sources of carbonaceous aerosols**

153 Seasonal average C_{EC} was 1.64 ± 0.84, 1.36 ± 0.57, 1.68 ± 0.81 and 1.70 ± 1.20
154 μgC/m^3, and that of C_{OC} was 5.17 ± 2.29, 4.70 ± 2.35, 6.49 ± 2.43 and 6.09 ± 2.64
155 μgC/m^3 in spring, summer, autumn and winter, respectively. Seasonal differences in
156 C_{EC} were very small among spring, autumn and winter, mainly due to the relatively

stable primary emissions of EC (e.g., vehicle exhaust) in these seasons in urban Guangzhou (Tao et al., 2017b). The lowest seasonal average C_{EC} and C_{OC} in summer were mainly due to the strongest diffusion (e.g., strongest solar radiation) and most frequent precipitation (**Fig. 2**). The highest seasonal average of C_{OC} in autumn might be related with, besides primary fossil combustion, the formation of secondary organic carbon due to the strong photochemical reaction and low precipitation in this season in the PRD region (Lu et al., 2021; Tao et al., 2014). Although the lowest mass concentration of $PM_{2.5}$ was also observed in summer (18.45 ± 5.48 μg/m^3), the highest one (53.52 ± 22.89 μg/m^3) was observed in winter rather than in autumn, suggesting the higher contribution of non-carbonaceous aerosols (e.g., secondary inorganic aerosols) to $PM_{2.5}$ in winter than autumn in this city (Tao et al., 2017a).

Moderate correlations ($R^2 \geq 0.58$, $p < 0.01$) between hourly C_{OC} and C_{EC} were found in all the seasons (**Fig. 3**), with the slopes of 2.3, 3.1, 2.7 and 1.9, in spring, summer, autumn and winter, respectively, implying the homogenic sources of carbonaceous aerosols in urban Guangzhou (Tao et al., 2017b). The relatively high slopes (OC/EC ratios) in the present study than reported previously for this city (Tao et al., 2014, 2017b) were likely due to the different method protocols (e.g., NIOSH-TOT protocol and IMPROVE-TOR protocol) (Cheng et al., 2011; Wu et al., 2016a). On average, the determined C_{EC} by IMPROVE-TOR protocol (denoted as $C_{EC\text{-}TOR}$) was 2.2 times of that by NIOSH-TOT protocol (denoted as $C_{EC\text{-}TOT}$) in urban areas in the PRD region (Wu et al., 2016a). The uncertainties in the above-mentioned factor of 2.2 should be less than 6% based on the range of the site-specific values which varied from 2.16 to 2.33 (Wu et al., 2016a). Taking into account this conversion factor, the seasonal slopes between C_{OC} and C_{EC} under the IMPROVE-TOR protocol in this study (**Appendix A Fig. S1**) are comparable to those (0.77–1.52) directly determined using IMPROVE-TOR protocol in previous studies (Tao et al., 2014, 2017b). The estimated OC/EC ratios under IMPROVE-TOR protocol are close to that of vehicle exhaust (1.1) and generally lower than those of coal combustion (2.7) and biomass burning (9.0)

(Watson et al., 2001). These values implied the predominant contribution of traffic emissions to carbonaceous aerosols in urban Guangzhou.

In addition, moderate correlations ($R^2 \geq 0.55$, $p < 0.01$) between hourly C_{EC} and NO_x ($NO+NO_2$) mixing ratio were found in all the seasons except summer (**Fig. 4**), further indicating the predominant contribution of traffic emissions to EC (Bos et al., 2021). The poor correlation between hourly C_{EC} and NO_x in summer was likely due to frequent rainfall, which removed particles more effectively than did insoluble gases (such as NO_x). A poor correlation was also found between hourly C_{EC} and C_{OC} in summer, likely due to two reasons. One is the excess OC from secondary aerosol formation, and another is the different precipitation scavenging efficiency between OC and EC due to their different size distributions (Tao et al., 2019).

2.2 Aerosol absorption coefficient and its wavelength dependence

b_{ap} at 950 nm ($b_{ap,950nm}$) showed a similar seasonal pattern to that of C_{EC} due to the predominant contribution of EC to aerosol light absorption at infrared wavelengths. The highest seasonal average of $b_{ap,950nm}$ was found in winter (10.43 ± 7.09 Mm^{-1}), which was 1.6 times of the lowest one in summer (6.50 ± 2.65 Mm^{-1}). Note that the average C_{EC} in winter is only 1.2 times of that in summer. The slightly different scales of seasonal variations between $b_{ap,950nm}$ and C_{EC} suggested other factors besides EC mass might also affect $b_{ap,950nm}$, e.g., coating fraction and coating thickness (Lack and Cappa, 2010; Lan et al., 2013; Zhang et al., 2018).

Wavelength dependence of b_{ap} could also be used to investigate the sources of carbonaceous aerosols. Generally, *AAE* has a value of around 1.0 in urban areas dominated by traffic emissions and a value larger than 1.6 dominated by biomass burning (Blanco-Alegre et al., 2020; Lack and Cappa, 2010). As shown in **Fig. 2b**, hourly $AAE_{370\text{-}950nm}$ varied in a range of 0.82–1.60 during the whole measurement period, likely indicating negligible contributions from biomass burning to b_{ap}.

Seasonal $AAE_{370\text{-}950nm}$ calculated from seasonally averaged b_{ap} at seven wavelengths using Eq. 4 was 1.07, 1.09, 1.19 and 1.17 in spring, summer, autumn and

winter, respectively, in urban Guangzhou (**Fig. 5**). $AAE_{370\text{-}950nm}$ values in all the seasons were evidently lower than those obtained in North China where atmospheric aerosols were largely affected by biomass burning and coal combustion emissions (Luo et al., 2021; Tian et al., 2020; Xia et al., 2020; Xie et al., 2019b). Brown carbon (BrC), which is mainly associated with biomass burning and coal combustion emissions, was estimated to contribute half of b_{ap} at UV wavelengths in winter in Beijing (Xie et al., 2019b; Wu et al., 2021). In these previous studies, a constant *AAE* of 1 for EC was generally used to segregate b_{ap} of BrC, which likely overestimated the contribution of BrC to b_{ap}. By coupling multiwavelength b_{ap} with chemical composition, Wang et al. (2021) estimated an average *AAE* of 1.19 for EC, a value that is the same as the highest seasonal average *AAE* in urban Guangzhou, suggesting negligible contributions of BrC from biomass burning and coal combustion to b_{ap} in this city. A modeling study by Zhang et al. (2020) showed *AAE* of EC with non-absorbing coatings in the range of 0.7–1.4. Thus, the slightly larger $AAE_{370\text{-}950nm}$ in autumn and winter than in spring and summer was likely due to the seasonal differences in EC morphology, size distribution and mixing state (Gyawali et al., 2012; Zhang et al., 2020).

AAE varied little with wavelength in the studied spectrum range. As shown in **Appendix A Fig. S2**, *AAE* in the short wavelength range of 370–590 nm ($AAE_{370\text{-}590nm}$), which is potentially affected by BrC (Cheng et al., 2016), is well consistent with that in the long wavelength range of 590–950 nm ($AAE_{590\text{-}950nm}$) which is little affected by BrC. The seasonal average $AAE_{370\text{-}590nm}$ was 1.13, 1.14, 1.24 and 1.26 in spring, summer, autumn and winter, respectively, which were only slightly higher than those (1.09, 1.12, 1.21 and 1.20) for $AAE_{590\text{-}950nm}$, further suggesting negligible contributions of BrC to b_{ap} in urban Guangzhou. The values of $AAE_{370\text{-}950nm}$ in the present study were consistent with previous results obtained in urban Guangzhou in 2015–2016 (Tao et al., 2021) and other cities in the PRD region, e.g., 1.1 in urban Shenzhen (Lan et al., 2013) and 1.0–1.1 in Hong Kong (Li et al., 2018). These results all indicated that EC was mainly emitted from vehicle emissions in the urban areas of the PRD region.

2.3 Seasonal variations in MAE_{EC} and influencing factors

Good correlations ($R^2 \geq 0.85$, $p < 0.01$)) were found between $b_{ap,950nm}$ and C_{EC} in four seasons (**Fig. 6**), indicating the dominant impact of EC mass on $b_{ap,950nm}$ at infrared wavelengths. Considering the negligible contribution of BrC to $b_{ap,950nm}$ at infrared wavelengths, the slope of zero-intercept linear regression of $b_{ap,950nm}$ against C_{EC} can be considered as the bulk MAE_{EC} at 950 nm ($MAE_{EC,950nm}$). The derived bulk $MAE_{EC,950nm}$ showed pronounced seasonal variations, with values of 6.13, 4.69, 5.44 and 5.97 m^2/g in spring, summer, autumn and winter, respectively, indicating seasonal variations in microphysical properties (e.g., mixing state, size distribution) of EC.

Bulk MAE_{EC} at 550 nm ($MAE_{EC,550nm}$), an intermediate wavelength in solar spectrum commonly concerned by previous studies (Bond and Bergstrom, 2006), can be estimated from $MAE_{EC,950nm}$ and seasonal *AAE* using Eq. (4). The derived $MAE_{EC,550nm}$ are 11.00, 8.51, 10.42 and 11.32 m^2/g in spring, summer, autumn and winter, respectively. These values are comparable to those obtained over the North China Plain (NCP) region. Based on the BC core size distribution and coating thickness measured by a single particle soot photometer (SP2), the *MAE* of coated BC at 550 nm was estimated to vary in a range of 8–12 m^2/g in the lower atmosphere over Beijing (Ding et al., 2019) and on a remote mountain in the NCP region (Ding et al., 2021). It should be noted that slightly higher *MAE* values in summer than winter were obtained over the NCP region (Ding et al., 2021) while the *MAE* was lowest in summer in urban Guangzhou. Higher *MAE* in summer over the NCP region was attributed to the smaller BC cores with higher absorbing capacity in this season compared to the case in winter. By contrast, EC was mainly emitted from vehicle emissions in urban Guangzhou, likely leading to a relatively invariant core size distribution throughout the year. The seasonal variations in *MAE* were thus mainly modulated by the coating extent. Compared to "pure EC" with a mean $MAE_{EC,550nm}$ of 7.5 m^2/g, seasonal $MAE_{EC,550nm}$ were enhanced by 47%, 13%, 39% and 51% in spring, summer autumn and winter, respectively (Bond and Bergstrom, 2006). The lowest enhancement in summer was likely due to a low

degree of coating of EC in this season. Low amplifications of *MAE* in summer (or wet season) were also found in previous studies in urban areas of the PRD region (Lan et al., 2013; Sun et al., 2020).

The amplifications of MAE_{EC} observed in the present study were comparable to those previously obtained in other urban regions worldwide (Andreae et al., 2008; Favez et al., 2009; Hu et al., 2020; Kondo et al., 2009; Lan et al., 2013; Liu et al., 2019; Ma et al., 2020; Sun et al., 2020; Wang et al., 2014, 2017, 2019; Wu et al., 2016b; Xie et al., 2019a, 2019b). Ma et al. (2020) observed a slightly wavelength-dependent absorption enhancement of 1.35–1.42 in Nanjing of the Yangtze River Delta region, which was attributed to the coating of particulate nitrate on BC particles from traffic emissions. Liu et al. (2019) found 1.4- and 1.6-times enhancements of BC absorption (870 nm) for summer and winter respectively in urban Beijing of the North China Plain region when $PM_1 > 50$ μg/m^3. Wang et al. (2014) obtained an average enhancement of 1.8 for BC absorption at 870 nm in a severely polluted urban region (Xi'an) of Northwest China. Generally, polluted environments combined with humid conditions are conducive to EC absorption enhancement by providing abundant secondary components for coating aged EC particles (Ma et al., 2020; Wang et al., 2020; Wu et al., 2016b; Zhang et al., 2020). The amplifications of MAE_{EC} in this study were also comparable to those obtained in urban Guangzhou in previous years of 2017–2018 presented by Sun et al. (2020), although a different approach named minimum R squared method was used to determine absorption enhancement in their study. However, increases in the MAE_{EC} enhancements were observed when compared to those obtained in all the seasons of 2015–2016 expect summer, likely related to the increasing nitrate fraction in $PM_{2.5}$ (Li et al., 2021). Increasing nitrate not only provided abundant materials for EC coatings but also increased aerosol hygroscopicity (Xu et al., 2020), which is further conducive to the internal mixing of EC with water-soluble matters (Tao et al., 2021).

Regarding diurnal pattern of MAE_{EC} in urban areas of the PRD region, a clear

297 afternoon peak was previously observed, corresponding well to the peak of number
298 fraction of core-shell mixed rBC particles out of total rBC-containing particles (an
299 indicator of rBC coating degree) and the peak of O_3 mixing ratio (Lan et al., 2013).
300 Thus, MAE_{EC} was considered to be largely affected by photochemical processes.
301 However, in the present study, no evident diurnal variations of MAE_{EC} were found in
302 any of the four seasons in urban Guangzhou, despite apparent afternoon peaks of
303 OC/EC ratio and O_3 concentration (**Fig. 7**). Note that hourly MAE_{EC} investigated in the
304 diurnal variations was calculated by hourly $b_{ap,950nm}$ divided by hourly C_{EC}. In addition,
305 no significant correlation (R^2=0.02) was found between daily $MAE_{EC,950nm}$ and OC/EC
306 ratio, implying limited influence of OC on the mixing state of EC in this city. A large
307 fraction of OC was attributed to secondary OC (SOC) mostly generated from gas-phase
308 reactions rather than heterogeneous reactions in urban Guangzhou (Chen et al., 2021),
309 implying SOC is likely externally mixed with EC, thereby has limited contribution to
310 the absorption enhancement of EC.

311 By contrast, daily $MAE_{EC,950nm}$ positively correlated with mass fraction of non-
312 carbonaceous aerosol components in $PM_{2.5}$ (R^2=0.60, $p < 0.01$) (**Fig. 8a**). Note that the
313 mass concentration of non-carbonaceous aerosol components is calculated as the
314 difference between $PM_{2.5}$ and the total of EC and organic matter (1.6×OC) (He et al.,
315 2011). Because the relatively low contributions of mineral aerosols and trace metals to
316 $PM_{2.5}$ in urban Guangzhou (Tao et al., 2014), the non-carbonaceous aerosol components
317 are mostly attributed to secondary inorganic aerosols (SIAs), such as sulfate, nitrate and
318 ammonium. The lowest $MAE_{EC,950nm}$ in summer was likely due to the lowest mass
319 fraction of non-carbonaceous aerosols in $PM_{2.5}$ (triangles in **Fig. 8a**). In addition, higher
320 $MAE_{EC,950nm}$ was also closely related with higher RH under the same mass fraction of
321 non-carbonaceous aerosols in $PM_{2.5}$ (**Fig. 8a**). High RH leads to high water content in
322 aerosols, which is conducive to EC core embedding into water-soluble SIA components.
323 Furthermore, high RH also favors the heterogeneous formation of SIAs on the surface
324 of EC particles, thereby increasing the probability of core-shell mixing (Wang et al.,

2020; Wu et al., 2016b; Zhang et al., 2020). Thus, ambient RH also plays a role on the variation of $MAE_{EC,950nm}$, which partly interpreted the relatively lower $MAE_{EC,950nm}$ in autumn (with low RH) than spring and winter, despite higher mass fraction of non-carbonaceous aerosol in autumn. In addition, daily $MAE_{EC,950nm}$ decreased with increasing mass fraction of EC in $PM_{2.5}$ (**Fig. 8b**), likely because a low fraction of EC in $PM_{2.5}$ was due to a high coating extent of EC by non-carbonaceous aerosols.

3 Conclusions

To investigate the seasonal variations of MAE_{EC} and associated dominant factors, hourly C_{EC}, C_{OC} and b_{ap} of $PM_{2.5}$ were simultaneously measured in urban Guangzhou in four seasons of 2018-2019. Moderate correlations between C_{EC} and C_{OC} were observed with low OC/EC mass ratios. C_{EC} also moderately correlated with NOx mixing ratio. In addition, the seasonal average *AAE* values were generally lower than 1.2 in all the seasons. These results demonstrated that carbonaceous aerosols were mainly from vehicle emissions in this city. In this environment dominated by traffic emissions, the estimated bulk $MAE_{EC,550nm}$ was 1.13-1.51 times of the mean value of 7.5 m^2/g commonly used for "pure EC". The high MAE_{EC} was determined by both SIAs and high ambient RH rather than potentially hydrophobic SOC. Results revealed that SIAs not only absorb moisture and increase the light scattering ability, but also enhance the light absorption ability of EC, further deteriorating the atmospheric visibility under the high ambient RH in the PRD region. Considering that the accuracy of MAE_{EC} is largely affected by the measurement methods for both C_{EC} and b_{ap}, measurements using advanced methods, e.g., photoacoustic soot spectrometer (PASS) for C_{EC} and SP2 for b_{ap}, are needed in the future to validate findings presented in this study.

Data availability. Data used in this study are available from Jun Tao (taojun@jnu.edu.cn).

Competing interests. The authors declare that they have no conflict of interest.

Acknowledgments

This work was supported by the National Natural Science Foundation of China (Nos. 41775155, 41875160 and 41475119).

Appendix A Supplementary data

Supplementary data associated with this article can be found in the online version at xxxxxx

References

Andreae, M.O., Gelencsér, A., 2006. Black carbon or brown carbon? The nature of light-absorbing carbonaceous aerosols. Atmos. Chem. Phys. 6, 3131–3148.

Andreae, M.O., Schmid, O., Yang, H., Chand, D., Yu, J.Z., Zeng, L.-M., et al., 2008. Optical properties and chemical composition of the atmospheric aerosol in urban Guangzhou, China. Atmos. Environ. 42, 6335–6350.

Birch, M.E., Cary, R.A., 1996. Elemental carbon-based method for monitoring occupational exposures to particulate diesel exhaust. Aerosol Sci. Technol. 25, 221–241.

Blanco-Alegre, C., Calvo, A.I., Alves, C., Fialho, P., Nunes, T., Gomes, J., et al., 2020. Aethalometer measurements in a road tunnel: A step forward in the characterization of black carbon emissions from traffic. Sci. Tot. Environ. 703, 135483.

Bond, T.C., Bergstrom, R.W., 2006. Light absorption by carbonaceous particles: An investigative review. Aerosol Sci. Technol. 40, 7–67.

Bond, T.C., Doherty, S.J., Fahey, D.W., Forster, P.M., Berntsen, T., Deangelo, B., et al., 2013. Bounding the role of black carbon in the climate system: A scientific assessment. J. Geophys. Res.-Atmos. 118, 5380–5552.

Bos, B., Lim, S., Hedges, M., Molden, N., Boyle, S., Mudway, D.I., et al., 2021. Taxi drivers' exposure to black carbon and nitrogen dioxide in electric and diesel vehicles: A case study in London. Environ. Res. 195, 110736.

Cappa, C.D., Onasch, T.B., Massoli, P., Worsnop, D.R., Bates, T.S., Cross, E.S., et al., 2012. Radiative absorption enhancements due to the mixing state of atmospheric

black carbon. Science 337, 1078–1081.

Cappa, C.D., Zhang, X., Russell, L.M., Collier, S., Lee, A.K.Y., Chen, C.-L., et al., 2019. Light absorption by ambient black and brown carbon and its dependence on black carbon coating state for two California, USA, cities in winter and summer. J. Geophys. Res.-Atmos. 124, 1550–1577.

Chen, W., Ye, Y.Q., Hu, W.W., Zhou, H.S., Pan, T.L., Wang, Y.K., et al., 2021. Real-time characterization of aerosol compositions, sources, and aging processes in Guangzhou during PRIDE-GBA 2018 campaign. J. Geophys. Res.-Atmos. 126, e2021JD035114.

Cheng, Y., Duan, F.-K., He, K.-B., Zheng, M., Du, Z.-Y., Ma, Y.-L., et al., 2011. Intercomparison of thermal–optical methods for the determination of organic and elemental carbon: influences of aerosol composition and implications. Environ. Sci. Technol. 45, 10117–10123.

Cheng, Y., He, K.-B., Du, Z.-Y., Engling, G., Liu, J.-M., Ma, Y.-L., et al., 2016. The characteristics of brown carbon aerosol during winter in Beijing. Atmos. Environ. 127. 355–364.

Ding, A.J., Huang, X., Nie, W., Sun, J.N., Kerminen, V.-M., Petäjä, T., et al., 2016. Enhanced haze pollution by black carbon in megacities in China. Geophys. Res. Lett. 43, 2873–2879.

Ding, S., Liu, D.T., Zhao, D.L., Hu, K., Tian, P., Zhou, W., et al., 2019. Size-related physical properties of black carbon in the lower atmosphere over Beijing and Europe. Environ. Sci. Technol. 53, 11112–11123.

Ding, S., Liu, D.T., Hu, K., Zhao, D.L., Tian, P., Wang, F., et al., 2021. Optical and hygroscopic properties of black carbon influenced by particle microphysics at the top of the anthropogenically polluted boundary layer. Atmos. Chem. Phys. 21, 681–694.

Favez, O., Alfaro, S.C., Sciare, J., Cachier, H., Abdelwahab, M.M., 2009. Ambient measurements of light-absorption by agricultural waste burning organic aerosols. J. Aerosol Sci. 40, 613–620.

Gyawali, M., Arnott, W.P., Zaveri, R.A., Song, C., Moosmüller, H., Liu, L., et al., 2012. Photoacoustic optical properties at UV, VIS, and near IR wavelengths for laboratory generated and winter time ambient urban aerosols. Atmos. Chem. Phys.

12, 2587–2601.

He, L.Y., Huang, X.F., Xue, L., Hu, M., Lin, Y., Zheng, J., et al., 2011. Submicron aerosol analysis and organic source apportionment in an urban atmosphere in Pearl River Delta of China using high-resolution aerosol mass spectrometry. J. Geophys. Res.-Atmos. 116, D12304.

Hu, K., Zhao, D.L., Liu, D.T., Ding, S., Tian, P., Yu, C.J., et al., 2020. Estimating radiative impacts of black carbon associated with mixing state in the lower atmosphere over the northern North China Plain. Chemosphere 252, 126455.

Jia, M.W., Evangeliou, N., Eckhardt, S., Huang, X., Gao, J., Ding, A.J., et al., 2021. Black carbon emission reduction due to COVID-19 lockdown in China. Geophys. Res. Lett. 48, e2021GL093243.

Kondo, Y., Sahu, L., Kuwata, M., Miyazaki, Y., Takegawa, N., Moteki, N., et al., 2009. Stabilization of the mass absorption cross section of black carbon for filter-based absorption photometry by the use of a heated inlet. Aerosol Sci. Technol. 43, 741–756.

Lack, D.A., Cappa, C.D., 2010. Impact of brown and clear carbon on light absorption enhancement, single scatter albedo and absorption wavelength dependence of black carbon. Atmos. Chem. Phys. 10, 4207–4220.

Lan, Z.-J., Huang, X.-F., Yu, K.-Y., Sun, T.-L., Zeng, .L-W., Hu, M., 2013. Light absorption of black carbon aerosol and its enhancement by mixing state in an urban atmosphere in South China. Atmos. Environ. 69, 118–123.

Li, G.-L., Sun, L., Ho, K.-F., Wong, K.-C., Ning, Z., 2018. Implication of light absorption enhancement and mixing state of black carbon (BC) by coatings in Hong Kong. Aerosol Air Qual. Res. 18, 2753–2763.

Li, J.W., Zhang, Z.S., Wu, Y.F., Tao, J., Xia, Y.J., Wang, C.Y., et al., 2021. Effects of chemical compositions in fine particles and their identified sources on hygroscopic growth factor during dry season in urban Guangzhou of South China. Sci. Tot. Environ. 801, 149749.

Liu, D.T., Joshi, R., Wang, J.F, Yu, C.J., Allan, J.D., Coe, H., et al., 2019. Contrasting physical properties of black carbon in urban Beijing between winter and summer. Atmos. Chem. Phys. 19, 6749–6769.

Lu, M.H., Zheng, J.Y., Huang, Z.J., Wu, C., Zheng, C.Z., Jia, G.L., et al., 2021. Insight

into the characteristics of carbonaceous aerosols at urban and regional sites in the downwind area of Pearl River Delta region, China. Sci. Tot. Environ. 778, 146251.

Luo, L.L., Tian, H.Z., Liu, H.J., Bai, X.X., Liu, W., Liu. S.H., et al., 2021. Seasonal variations in the mass characteristics and optical properties of carbonaceous constituents of $PM_{2.5}$ in six cities of North China. Environ. Pollut. 268(PartB), 115780.

Ma, Y., Huang, C., Jabbour, H., Zheng, Z., Wang, Y., Jiang, Y., et al., 2020. Mixing state and light absorption enhancement of black carbon aerosols in summertime Nanjing, China. Atmos. Environ. 222, 117141.

Peng, J., Hu, M., Guo, S., Du, Z., Zheng, J., Shang, D., et al., 2016. Markedly enhanced absorption and direct radiative forcing of black carbon under polluted urban environments. Proc. Natl. Acad. Sci. U.S.A. 113, 4266–4271.

Sun, J.Y., Wu, C., Wu, D., Cheng, C., Li, M., Li, L., et al., 2020. Amplification of black carbon light absorption induced by atmospheric aging: temporal variation at seasonal and diel scales in urban Guangzhou. Atmos. Chem. Phys. 20, 2445–2470.

Tao, J., Zhang, L., Ho, K., Zhang, R., Lin, Z., Zhang, Z., et al., 2014. Impact of $PM_{2.5}$ chemical compositions on aerosol light scattering in Guangzhou - the largest megacity in South China. Atmos. Res.135–136, 48–58.

Tao, J., Zhang, L., Cao, J., Zhang, R., 2017a. A review of current knowledge concerning $PM_{2.5}$ chemical composition, aerosol optical properties and their relationships across China. Atmos. Chem. Phys. 17, 9485–9518.

Tao, J., Zhang, L., Cao, J., Zhong, L., Chen, D., Yang, Y., et al., 2017b. Source apportionment of $PM_{2.5}$ at urban and suburban areas of the Pearl River Delta region, South China - With emphasis on ship emissions. Sci. Tot. Environ. 574, 1559–1570.

Tao, J., Zhang, Z.S., Wu, Y.F., Zhang, L.M., Wu, Z.J.,Cheng, P., et al., 2019. Impact of particle number and mass size distributions of majorchemical components on particle mass scattering efficiency in urban Guangzhou in southern China. Atmos. Chem. Phys. 19, 8471–8490.

Tao, J., Zhang, L., Wu, Y., Zhang, Z., 2020. Evaluation of the IMPROVE formulas based on Mie model in the calculation of particle scattering coefficient in an urban atmosphere. Atmos. Environ. 222, 117116.

Tao, J., Zhang, Z., Zhang, L., Wu, Y., Zhang, R., Wang, B., 2021. Impact of deliquescence of aerosol on mass absorption efficiency of elemental carbon in fine particles in urban Guangzhou in south China. Atmos. Environ. 256, 118476.

Tian, P., Liu, D.T., Zhao, D.L., Yu, C.J., Liu, Q., Huang, M.Y., et al., 2020. In situ vertical characteristics of optical properties and heating rates of aerosol over Beijing. Atmos. Chem. Phys. 20, 2603–2622.

Wang, J.F., Zhang, Q., Chen, M.D., Collier, S., Zhou, S., Ge, X.L., et al., 2017. First chemical characterization of refractory black carbon aerosols and associated coatings over the Tibetan Plateau (4730 m asl). Environ. Sci. Technol. 51(24), 14072–14082.

Wang, J.F., Liu, D.T., Ge, X.L., Wu, Y.Z., Shen, F.Z., Chen, M.D., et al., 2019. Characterization of black carbon-containing fine particles in Beijing during wintertime. Atmos. Chem. Phys. 19, 447–458.

Wang, J.F., Li, J.Y., Ye, J.H., Zhao, J., Wu, Y.Z., Hu, J.L., et al., 2020. Fast sulfate formation from oxidation of SO_2 by NO_2 and HONO observed in Beijing haze. Nat. Commun. 11, 2844.

Wang, Q.Y., Huang, R-J, Cao, J.J., Han, Y.M., Wang, G.H., Li, G.H, et al., 2014. Mixing state of black carbon aerosol in a heavily polluted urban area of China: Implications for light absorption enhancement. Aerosol Sci. Technol. 48, 689–697.

Wang, Q.Y., Liu, H.K., Ye, J.H., Tian, J., Zhang, T., Zhang, Y., et al., 2021. Estimating absorption Ångström exponent of black carbon aeorosl by coupling multiwavelength absorption with chemical composition. Environ. Sci. Technol. Lett. 8(2), 121–127.

Watson, J.G., Chow, J.C., Houck, J.E., 2001. $PM_{2.5}$ chemical source profiles for vehicle exhaust, vegetative burning, geological material, and coal burning in Northwestern Colorado during 1995. Chemosphere 43, 1141–1151.

Weingartner, E., Saathoff, H., Schnaiter, M., Streit, N., Bitnar, B., Baltensperger, U., 2003. Absorption of light by soot particles: determination of the absorption coefficient by means of aethalometers. J. Aerosol Sci. 34, 1445–1463.

Wu, C., Huang, X.H.H., Ng, W.M., Griffith, S.M., Yu, J.Z., 2016a. Inter-comparison of NIOSH and IMPROVE protocols for OC and EC determination: implications for inter-protocol data conversion. Atmos. Meas. Tech. 9, 4547–4560.

512 Wu, Y.F., Zhang, R.J., Tian, P., Tao, J., Hsu, S.-C., Yan, P., et al., 2016b. Effect of
513 ambient humidity on the light absorption amplification of black carbon in Beijing
514 during January 2013. Atmos. Environ. 124, 217–223.
515 Wu, Y.F., Li, J.W., Jiang, C., Xia, Y.J., Tao, J., Tian, P., et al., 2021. Spectral absorption
516 properties of organic carbon aerosol during a polluted winter in Beijing, China.
517 Sci. Tot. Environ. 755, 142600.
518 Xia, Y.J., Wu, Y.F., Huang, R.-J., Xia, X.A., Tang, J., Wang, M., et al., 2020. Variation
519 in black carbon concentration and aerosol optical properties in Beijing: Role of
520 emission control and meteorological transport variability. Chemosphere 254,
521 126849.
522 Xie, C.H., Xu, W.Q., Wang, J.F., Liu, D.T., Ge, X.L., Zhang, Q.,et al., 2019a. Light
523 absorption enhancement of black carbon in urban Beijing in summer. Atmos.
524 Environ. 213, 499–504.
525 Xie, C.H., Xu, W.Q., Wang, J.F., Wang, Q.Q., Liu, D.T., Tang, G.Q., et al., 2019b.
526 Vertical characterization of aerosol optical properties and brown carbon in winter
527 in urban Beijing, China. Atmos. Chem. Phys. 19, 165–179.
528 Xu, Y.W., Kuang, Y., Bian, Y.X., Liu, L., Li, F., Wang, Y.Q., et al., 2020. Current
529 changllenges in visibility improvement in Southern China. Environ. Sci. Technol.
530 Lett. 7(6), 395–401.
531 Zhang, F., Wang, Y., Peng, J.F., Chen, L., Sun, Y.L., Duan, L., et al., 2020. An
532 unexpected catalyst dominates formation and radiative forcing of regional haze.
533 Proc. Natl. Acad. Sci. U.S.A.117, 3960–3966.
534 Zhang, X.L, Mao, M., Yin, Y., Tang, S.H., 2020. The absorption Ångstrom exponent of
535 black carbon with brown coatings: effects of aerosol microphysics and
536 parameterization. Atmos. Chem. Phys. 20, 9701–9711.
537 Zhang, X.L., Mao, M., Yin, Y., Wang, B., 2017. Absorption enhancement of aged black
538 carbon aerosols affected by their microphysics: A numerical investigation. J Quant.
539 Spectrosc. Radiat. Transf. 202, 90–97.
540 Zhang, Y.X., Zhang, Q., Cheng, Y.F., Su, H., Li, H.Y., Li, M., et al., 2018. Amplification
541 of light absorption of black carbon associated with air pollution. Atmos. Chem.
542 Phys. 18, 9879–9896.
543 Zhao, C.F., Yang, Y.K., Fan, H., Huang, J.P., Fu, Y.F., Zhang, X.Y., et al., 2020. Aerosol

544 characteristics and impacts on weather and climate over the Tibetan Plateau. Natl.
545 Sci. Rev. 7, 492–495.

List of Figures

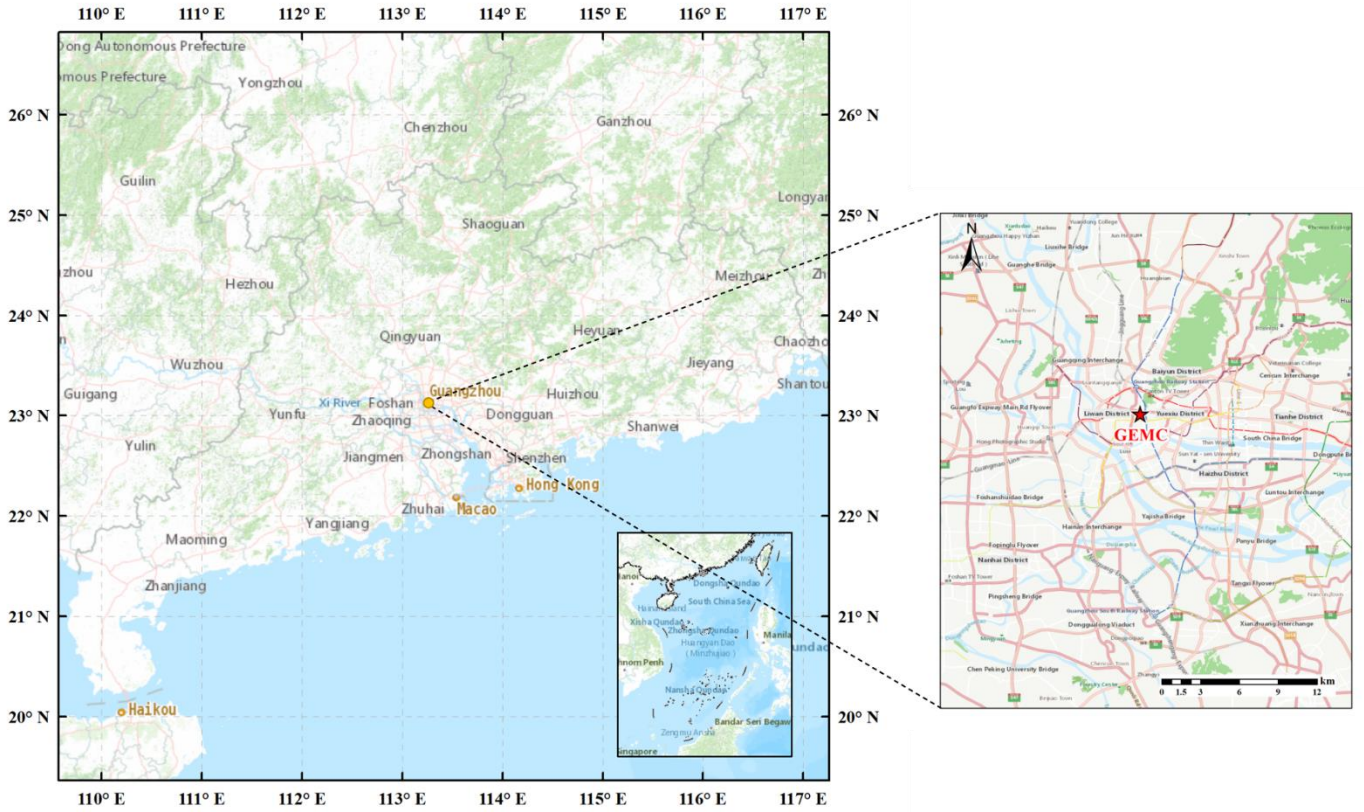
110° E
111° E
112° E
113° E
114° E
115° E
116° E
117° E
26° N
25° N
24° N
23° N
22° N
21° N
20° N
Yongzhou
Chenzhou
Ganzhou
Guilin
Shaoguan
Hezhou
Meizhou
Qingyuan
Heyuan
Jieyang
Wuzhou
Guigang
Guangzhou
Huizhou
Xi River
Foshan
Yunfu
Zhaoqing
Dongguan
Shanwei
Yulin
Jiangmen
Zhongshan
Shenzhen
Hong Kong
Zhuhai
Macao
Yangjiang
Maoming
Zhanjiang
Haikou
N
GEMC
km
0 1.5 3 6 9 12

Fig.1

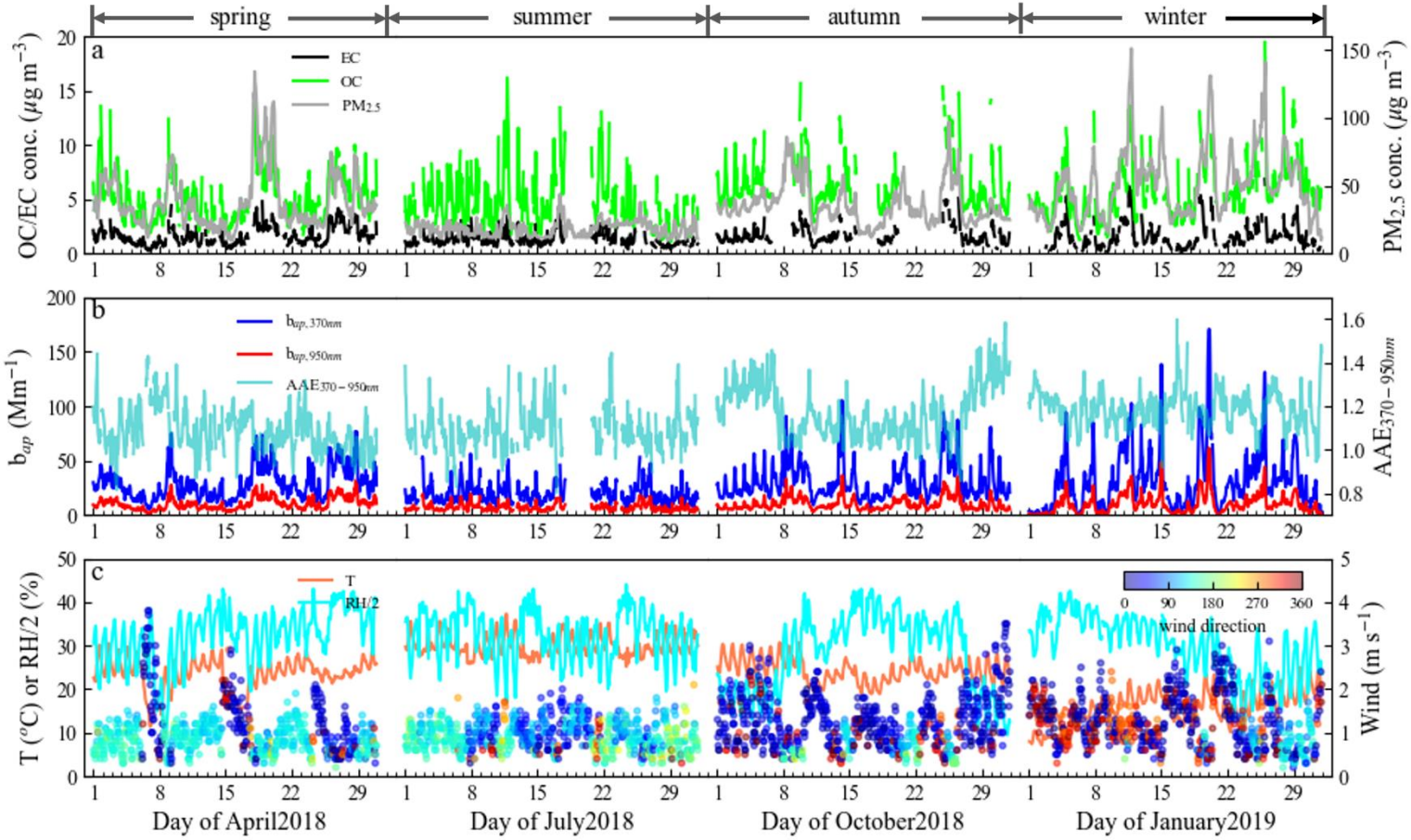
spring
summer
autumn
winter
a
EC
OC
PM2.5
OC/EC conc. (μg m−3)
PM2.5 conc. (μg m−3)
b
bap,370nm
bap,950nm
AAE370−950nm
bap (Mm−1)
AAE370−950nm
c
T
RH/2
0 90 180 270 360
wind direction
T (°C) or RH/2 (%)
Wind (m s−1)
Day of April2018
Day of July2018
Day of October2018
Day of January2019

Fig.2

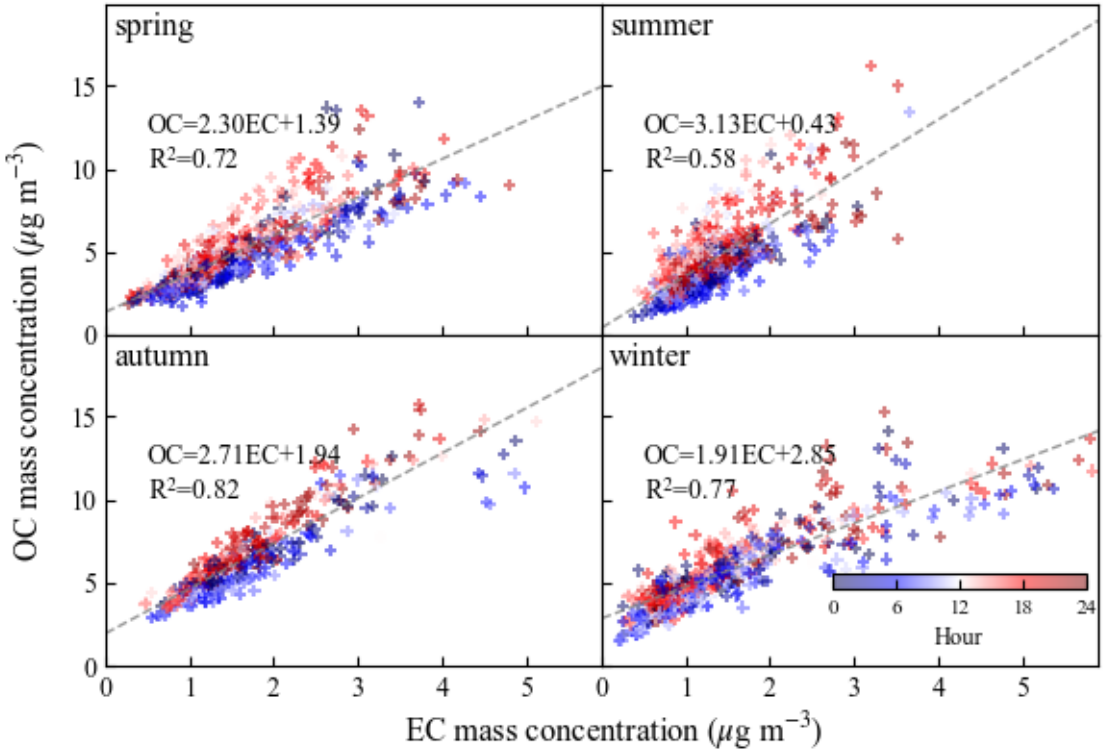
spring
OC=2.30EC+1.39
R²=0.72
summer
OC=3.13EC+0.43
R²=0.58
autumn
OC=2.71EC+1.94
R²=0.82
winter
OC=1.91EC+2.85
R²=0.77
0
6
12
18
24
Hour
OC mass concentration (μg m⁻³)
EC mass concentration (μg m⁻³)
0
5
10
15
0
1
2
3
4
5

Fig.3

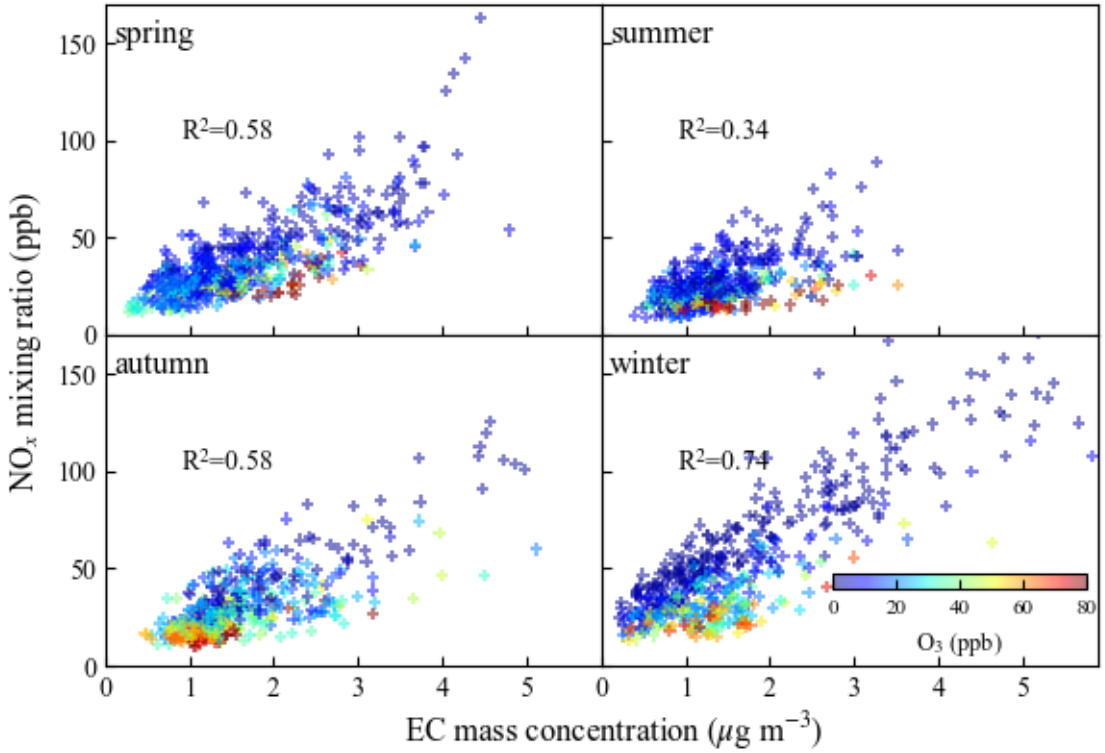
spring
summer
autumn
winter
R²=0.58
R²=0.34
R²=0.58
R²=0.74
NOx mixing ratio (ppb)
EC mass concentration (μg m⁻³)
O3 (ppb)
0
20
40
60
80

Fig.4

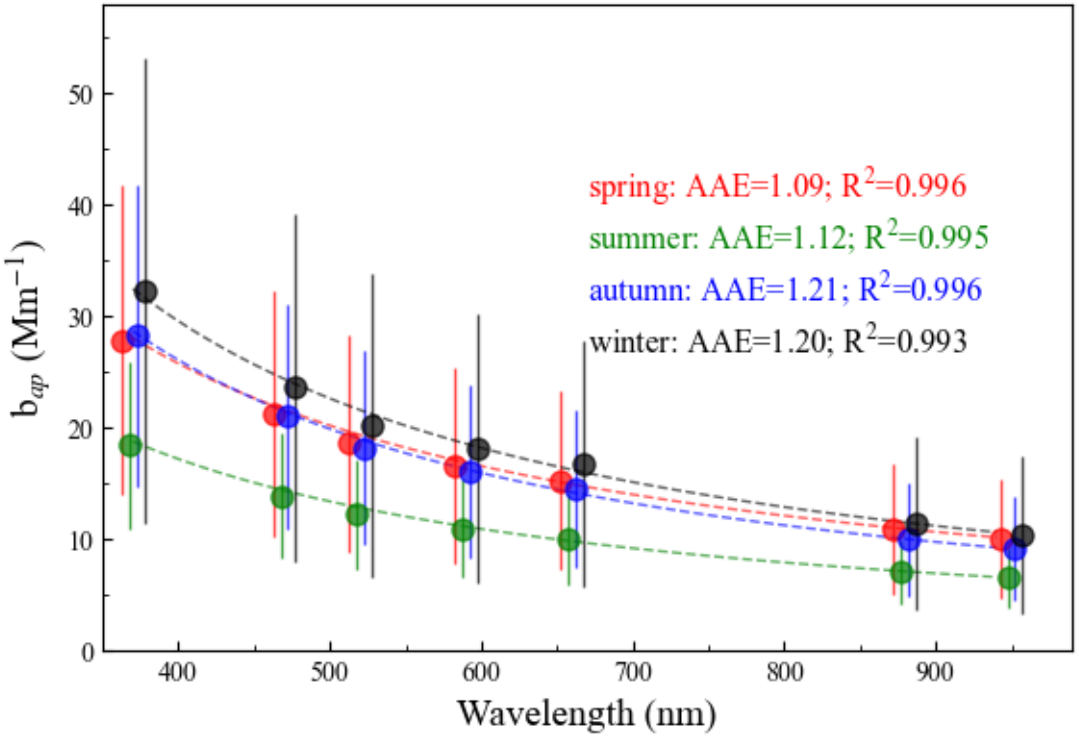
spring: AAE=1.09; R2=0.996
summer: AAE=1.12; R2=0.995
autumn: AAE=1.21; R2=0.996
winter: AAE=1.20; R2=0.993
bap (Mm-1)
Wavelength (nm)
0
10
20
30
40
50
400
500
600
700
800
900

Fig.5

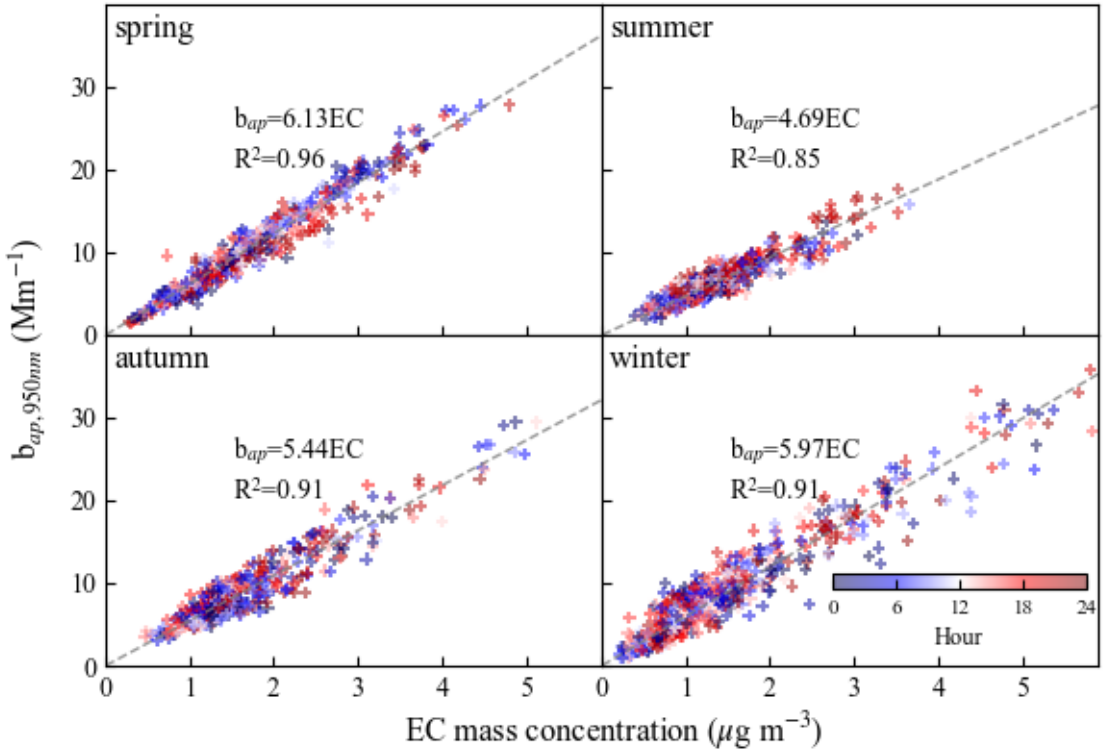
spring
summer
autumn
winter
b_{ap}=6.13EC
R^2=0.96
b_{ap}=4.69EC
R^2=0.85
b_{ap}=5.44EC
R^2=0.91
b_{ap}=5.97EC
R^2=0.91
0
6
12
18
24
Hour
$b_{ap,950nm}$ (Mm^{-1})
EC mass concentration (μg m^{-3})

Fig.6

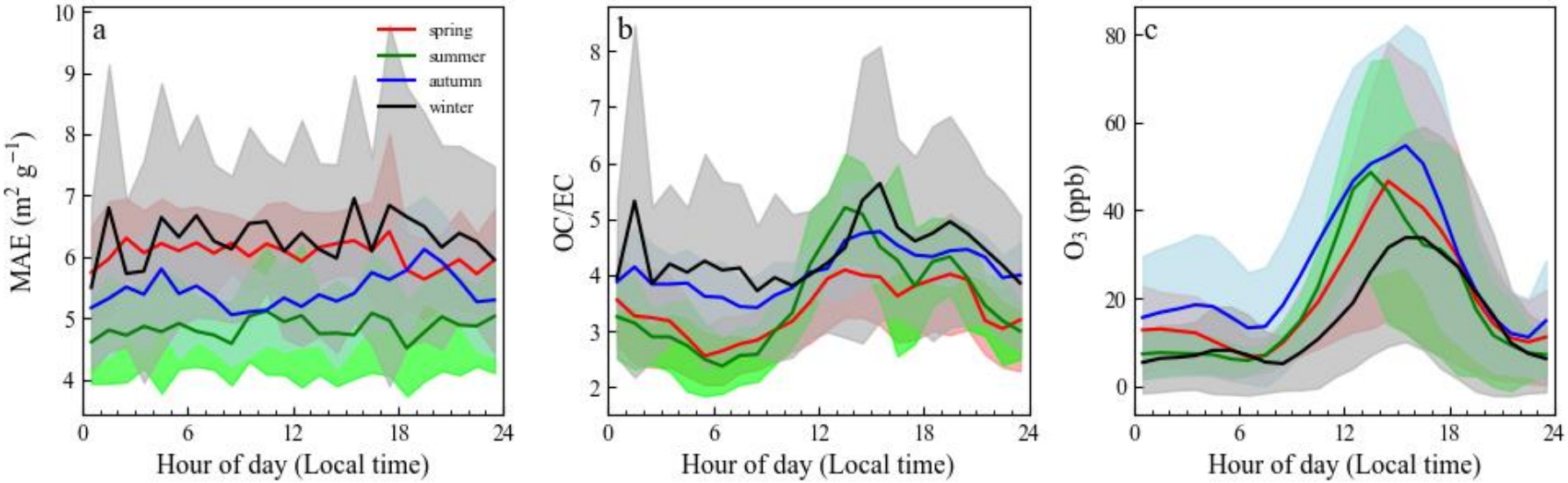
a
spring
summer
autumn
winter
MAE (m^2 g^{-1})
Hour of day (Local time)
b
OC/EC
Hour of day (Local time)
c
O_3 (ppb)
Hour of day (Local time)

Fig.7

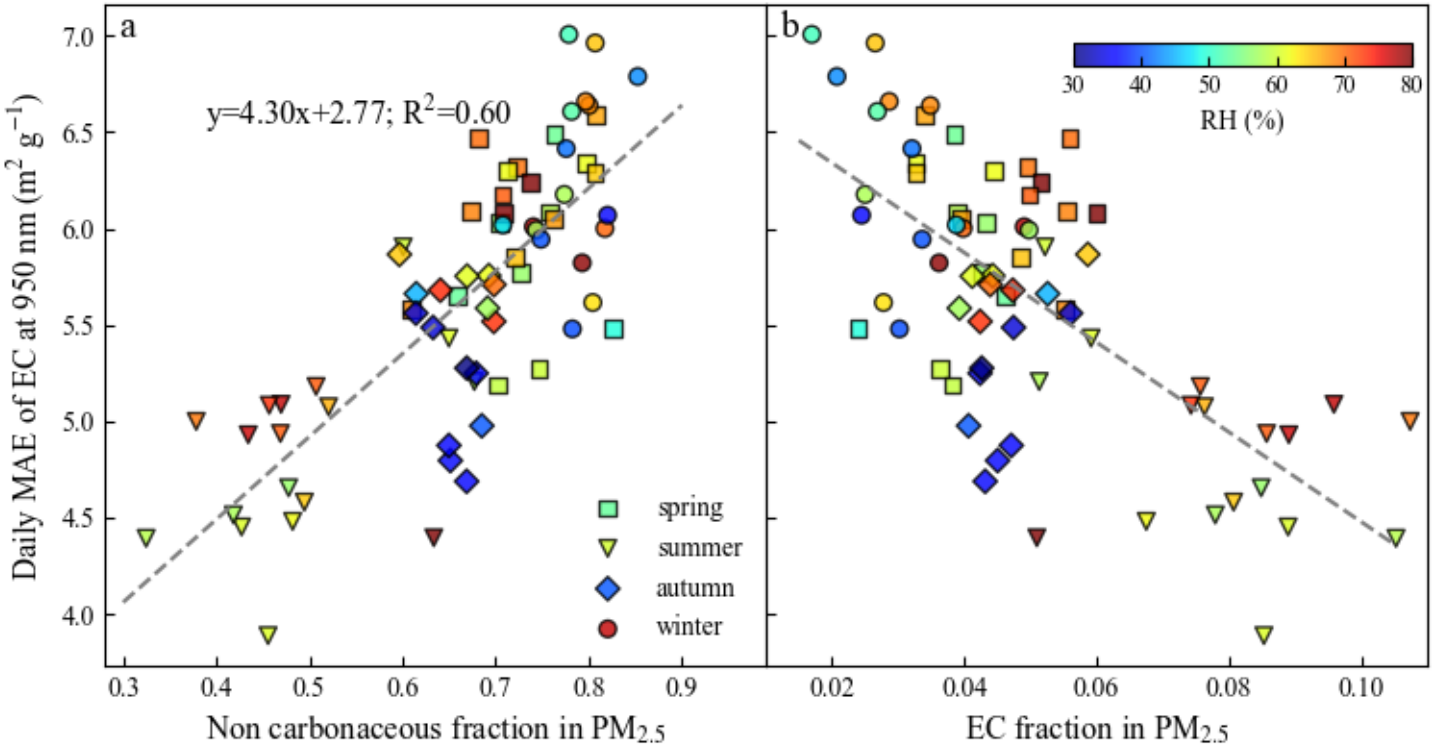
a
b
y=4.30x+2.77; R2=0.60
Daily MAE of EC at 950 nm (m2 g-1)
Non carbonaceous fraction in PM2.5
EC fraction in PM2.5
RH (%)
spring
summer
autumn
winter

Fig.8

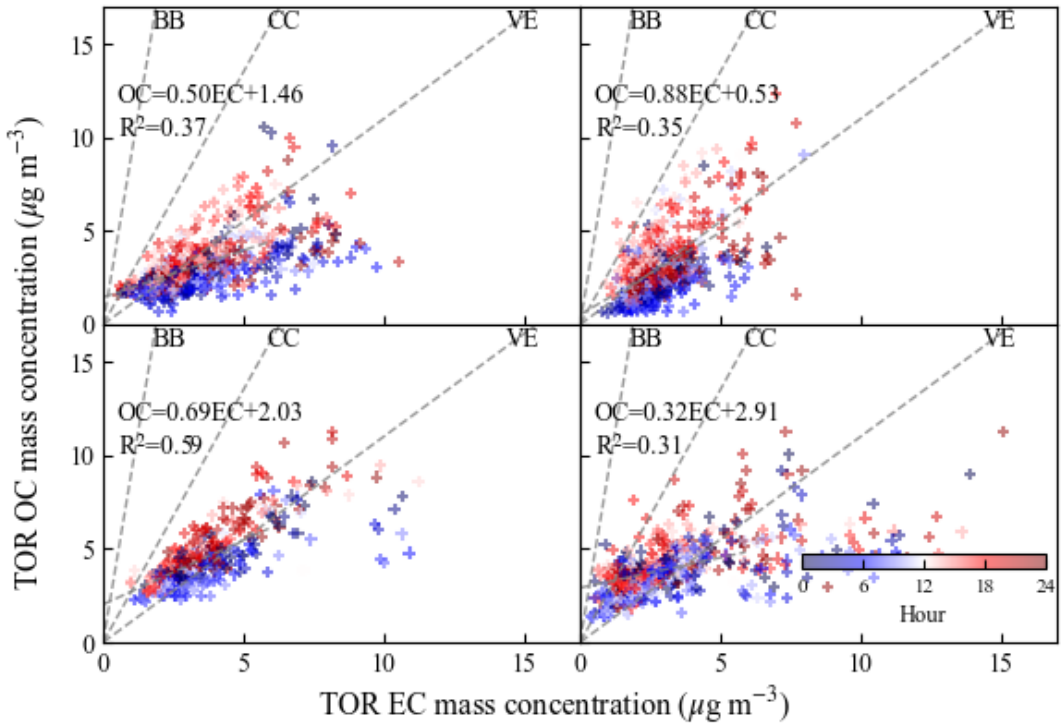

Fig. S1 Scatter plots of hourly mass concentration of OC versus EC under the IMPROVE-TOR protocol in four seasons. The TOR EC mass concentrations were calculated from the measured EC mass concentrations using the NIOSH-TOT protocol by considering a conversion factor of 2.2 proposed by Wu et al. (2016). The TOR OC mass concentrations were then calculated by subtracting the TOR EC mass concentrations from the total carbon mass concentrations, which are the sum of measured OC and EC concentrations. Dashed lines represent the typical TOR OC/EC mass ratios for biomass burning (BB, 9), coal combustion (CC, 2.7) and vehicle exhaust (VE, 1.1), respectively, proposed by Waston et al. (2001).

References

Wu, C, Huang, X H H, Ng, W M, Griffith, S M, Yu, J Z, 2016a. Inter-comparison of NIOSH and IMPROVE protocols for OC and EC determination: implications for inter-protocol data conversion. Atmos. Meas. Tech. 9:4547-4560.

Watson, J G, Chow, J C, Houck, J E, 2001. $PM_{2.5}$ chemical source profiles for vehicle exhaust, vegetative burning, geological material, and coal burning in Northwestern Colorado during 1995. Chemosphere 43:1141-1151.

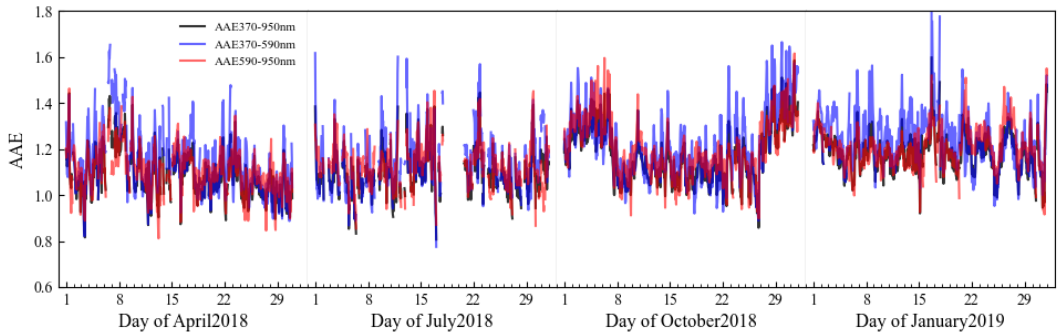

Fig. S2 Hourly variations of *AAE* in the wavelength range of 370–950 nm (black line), and two sub-ranges of 370–590 nm (blue line) and 590–950 nm (red line).